GRAVITY FIELD OF THE LUNAR SOUTH POLE FROM GRAIL MISSION DATA. Sander Goossens[1,2], Terence J. Sabaka[2], Mark A. Wieczorek[3], Gregory A. Neumann[2], Erwan Mazarico[2], Frank G. Lemoine[2], Joseph B. Nicholas[2,4], David E. Smith[5], Maria T. Zuber[5]. [1]Center for Research and Exploration in Space Science and Technology, University of Maryland Baltimore County, 1000 Hilltop Circle, Baltimore MD 21250 U.S.A. (email: sander.j.goossens@nasa.gov), [2]NASA Goddard Space Flight Center, 8800 Greenbelt Road, Greenbelt MD 20771 U.S.A., [3]Université Côte d'Azur, Observatoire de la Côte d'Azur, CNRS, Laboratoire Lagrange, Nice, France, [4]Emergent Space Technologies, 6411 Ivy Lane, Greenbelt, MD 20770, U.S.A., [5]Massachusetts Institute of Technology, 77 Massachusetts Avenue, Cambridge MA 02139 USA.

Introduction: The Gravity Recovery and Interior Laboratory (GRAIL) mission to the Moon was designed to determine the structure of the lunar interior from crust to core and to advance the understanding of the thermal evolution of the Moon [1,2], by producing a high-quality, high-resolution map of the gravitational field of the Moon. GRAIL's science data consist of precise measurements of the distance between two co-orbiting satellites using a Ka-band ranging system [3], augmented by tracking from Earth using the Deep Space Network [4]. Analysis of GRAIL data has resulted in several high-resolution global gravity field models expressed in spherical harmonics, the most recent of which have a maximum degree and order of 1200 [5] or 1500 [6]. In addition to global models, local models have also been determined [7].

As the resolution of the GRAIL gravity models improved, high correlations between gravity and topography (from the Lunar Orbiter Laser Altimeter LOLA onboard LRO [8]) were obtained at smaller and smaller scales. Yet at degrees larger than the range 600-700, the global correlations between gravity and topography for the models decrease rapidly with increasing degree, and this limits the use of these models for geophysical analysis to only those degrees where the correlations are still deemed high enough.

With the recent focus on the lunar south pole area in the framework of the return to the lunar surface in 2024, we present results for the gravity field of the lunar south pole from our recent global model [9], as well as results from a local analysis [10]. We interpret the results in terms of models of the density of the lunar crust. New models of the density of the crust in the south pole area can help inform the site assessment of future landing site candidates.

Methods: We have reanalyzed the GRAIL data to estimate a gravity field model of degree and order 1200 in spherical harmonics. We apply a constraint based on topography information, that results in high correlations between gravity and topography by design, and that allows for a direct determination of the bulk crustal density [11]. To validate the results from a model with this new constraint, we applied it to a pre-GRAIL data system and showed that we obtain the same bulk crustal density estimate for this model as was obtained from GRAIL data. We then use the new model to estimate the lateral and vertical density structure of the lunar crust, following earlier work by *Besserer et al.* (2014) [12] and *Han et al.* (2014) [13]. With our new model, we can increase the resolution when compared to these earlier results. In addition, we will also present gravity field models of the south pole using a local approach [9,12].

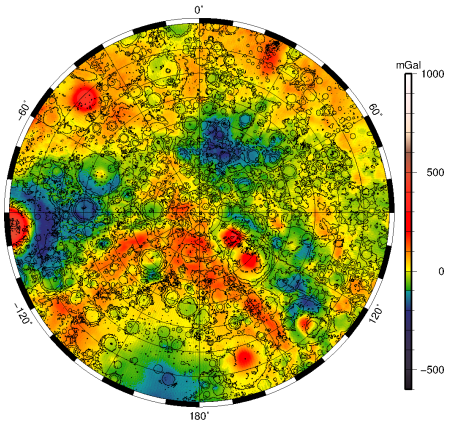

Figure 1 Bouguer anomalies for our new model, using a constant crustal density of 2500 kg m^{-3} [cf. 16]. The map is in stereographic projection centered on the south pole, and shows the Bouguer anomalies to a latitude of 50˚S. Topography contours at an interval of 2 km are included for context. Bouguer anomalies were computed between spherical harmonic degrees 7 and 900.

Results: In Figure 1, we show Bouguer anomalies for our new model. We used a constant crustal density of 2500 kg m^{-3} to construct the Bouguer anomalies. Variations in Bouguer anomalies map indicate density variations in the crust. The anomalies in Figure 1 were expanded between degrees 7 and 900, with the lower bound chosen so that the anomalies shown are not dominated by the strong signal from the lower degrees. Our new constraint allows us to extend the range to about 900 without introducing noisy patterns.

We show localized correlations between gravity and topography-induced gravity (computed following *Wieczorek and Phillips* (1998) [14]) in Figure 2. We localize by multiplying the data with specially con-

structed localization windows using a spherical cap radius of 7.5˚ (centered on the south pole) and a bandwidth of L_{win}= 116 [15]. We average the results from the first 30 tapers with the highest concentration [9,15]. The correlations for our new model with the topography constraint are higher than those for a model with the standard Kaula constraint, by design. In Figure 2 we also include the effective density spectrum, which is a measure of crustal density at different spatial scales [12,13,16].

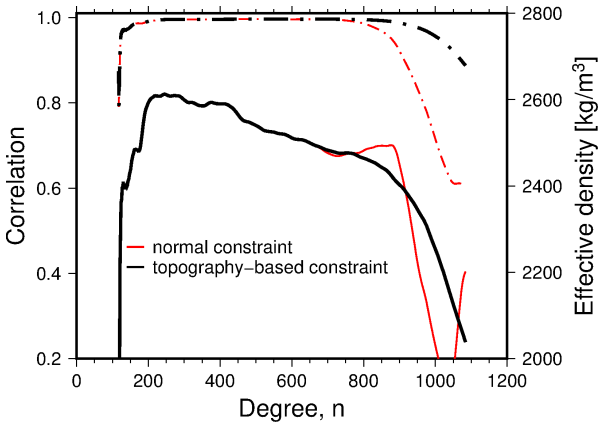

Figure 2 Localized correlations (dash-dot) and effective density spectra (solid) for a model with a normal (Kaula) constraint, and for a model with our new, topography-based constraint. The localization is centered on the south pole, using a spherical cap with a radius of 7.5˚.

Localized effective density spectra can be used to estimate parameters of a model of vertical density variations. We estimated parameters for a linear model (a surface density and a linear gradient) and an exponential model (a surface density and an e-fold depth). Improved localized correlations imply that more spherical harmonic degrees can be used to determine the parameters of the density model, thus improving the estimates. Figure 2 indeed shows a more stable effective density spectrum for our new model.

In Figures 3 and 4 we show results for the surface density and gradient for the linear model, respectively. Local spectra were computed as in Figure 2, at grid points spaced 5˚, after which the results were interpolated for mapping purposes. Surface densities are on average low. Lower surface densities can be translated into higher porosity. Several areas have higher densities, especially in the south pole-Aitken area. Patches of lower than average densities also exist. The gradients are in general positive, with some areas with negative gradients (density inversions) also present.

References: [1] Zuber M. T. *et al*. (2012), *Science*, doi: 10.1126/ science.1231507. [2] Zuber M. T. *et al*. (2013), *Space Sci. Rev*. doi:10.1007/s11214-012-9952-7. [3] Klipstein W.M. *et al*. (2013), *Space Sci. Rev*.

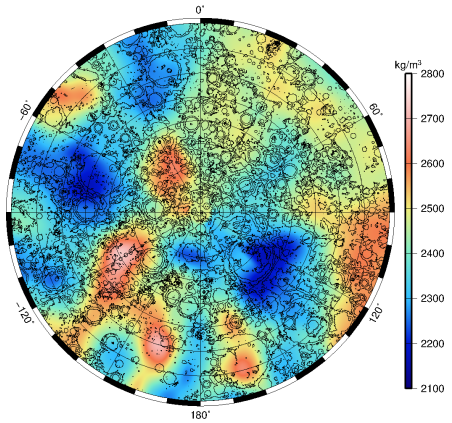

Figure 3 Surface density from a fit of a linear density-depth model, using the degree range n = 250-650. The map projection is the same as in Figure 1.

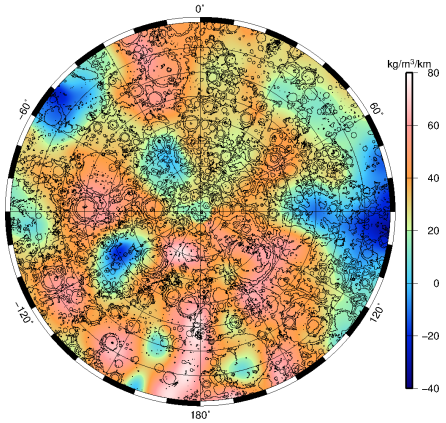

Figure 4 Density gradients for a fit of a linear density-depth model, using the degree range n = 250-650. The map projection is again the same as in Figure 1.

doi:10.1007/s11214-013-9973-x . [4] Asmar S.W. *et al*. (2013), *Space Sci. Rev*. doi:10. 1007/s11214-013-9962-0. [5] Goossens S. *et al*. (2016), 47th LPSC, abstract 1484. 68] Park R. S. *et al*. (2015), *AGU Fall Meeting*, paper G41B-01. [7] Goossens S. *et al*. (2014), *Geophys. Res. Lett*., doi: 10.1002/2014GL060178. [8] Smith D. E. *et al*. (2017), *Icarus,* doi:10.1016/j.icarus. 2016.06.006. [9] Goossens S. *et al*. (2020), *J. Geophys. Res. Planets*, doi: 10.1029/2019JE006086. [10] Goossens S. *et al*. (2018), 49th LPSC, abstract 2477. [11] Goossens S. *et al*. (2017), *Geophys. Res. Lett*., doi: 10.1002/2017GL074172. [12] Besserer J. *et al.* (2014), *Geophys. Res. Lett*., doi: 10.1002/2014GL060240. [13] Han S.-C. *et al*. (2014), *Geophys. Res. Lett*., doi: 10.1002/2014GL059378. [14] Wieczorek M.A. and Phillips R.J. (1998), *J. Geophys. Res*., doi: 10.1029/97JE03136. [15] Wieczorek M.A. and Simons F.J. (2005), *Geophys. J. Int*., doi: 10.1111/j.1365-246X. 2005.02687.x. [16] Wieczorek M.A. *et al., Science,* doi:10.1126/science.1231530.